GEOCHEMISTRY, MINERALOGY AND PETROLOGY • SOFIA
ГЕОХИМИЯ, МИНЕРАЛОГИЯ И ПЕТРОЛОГИЯ • СОФИЯ
2007, **45**, 79-95.

Amphibole-bearing leucosome from the Chepelare area, Central Rhodopes: P-T conditions of melting and crystallization

Zlatka Cherneva, Milena Georgieva

Abstract. Undeformed leucosome in migmatitic amphibole-biotite gneisses contains large (2-3 cm) euhedral poikilitic amphibole. The leucosome matrix (felsic minerals surrounding amphibole grains) comprises relatively equal proportions of plagioclase, K-feldspar and quartz. Grain scale relations indicate a simultaneous crystallization of major minerals with some priority to amphibole. Amphibole-plagioclase thermobarometry and two-feldspar thermometry define a *P-T*-path of anatectic melt crystallization in the sillimanite stability field from 760˚C/0.8 GPa to 650˚C/0.8-0.6 GPa, followed by feldspars subsolidus re-equilibration at 550-450˚C. Garnet-kyanite bearing leucosomes in neighbouring pelitic gneisses and schists corroborate inferred hypothesis of fluid-present melting reactions, involving biotite breakdown at upper amphibolite to moderate-pressure granulite facies transition (>760˚C/>1 GPa). The thermobarometric estimates do not specify the thermal peak of melting. They rather expand the *P-T* field of migmatization in the Central Rhodope Arda unit towards a higher-grade facies.

Key words: migmatites, melting, amphibole-bearing leucosome, thermobarometry, Central Rhodopes

Addresses: Z. Cherneva - Sofia University "St Kliment Ohridski", 1504 Sofia; Geological Institute, Bulgarian Academy of Sciences, 1113 Sofia; E-mail: cherneva@gea.uni-sofia.bg; M. Georgieva - Sofia University "St Kliment Ohridski", 1504 Sofia

Златка Чернева, Милена Георгиева. Амфибол-съдържаща левкосома от района на Чепеларе, Централни Родопи: P-T условия на топене и кристализация

Резюме. Недеформирана левкосома в мигматични амфибол-биотитови гнайси съдържа едър (2-3 cm) автоморфен амфибол. Матриксът (салични минерали около амфиболовите зърна) е изграден от приблизително еднакви количества плагиоклаз, К-фелдшпат и кварц. Микроструктурните отношения показват едновременна кристализация на мине-ралите с известно предимство за амфибола. Резултатите от амфибол-плагиоклазова термобарометрия и двуфелдшпатова термометрия характеризират *P-T* условията на кристализация на анатектичната топилка в полето на стабилност на силиманита от 760˚C/0,8 GPa до 650˚C/0,8-0,6 GPa, последвана от субсолидусно преуравновесяване на фелдшпатите при 550-450˚C. Присъствието на гранат-кианит-съдържащи левкосоми в съседни пелитови гнайси и

шисти подкрепя идеята за реакции на топене с участие на биотит и привнос на флуид в условия на преход от висок амфиболитов към умеренобаричен гранулитов фациес (> 760˚C/> 1 GPa). Резултатите от изследването не характери-зират термалния пик на топене. Те разширяват към по-висок фациес *P-T* областта на проява на мигматизация в единицата Арда в Централните Родопи.

Introduction

Mafic minerals in migmatites are indicative of melting reactions and *P-T* conditions of melting. Prominent among them are the anhydrous silicates like garnet and pyroxene produced as peritectic phases together with anatectic melts. Amphibole behavior at crustal melting conditions gives rise to considerable interest in understanding the generation of granodioritic and tonalitic melts. The presence of amphibole in the neosome of migmatitic biotite- and amphibole-biotite gneisses refers to biotite incongruent melting (Büsch et al., 1974; Lappin, Hollister, 1980; Kenah, Hollister, 1983; Mogk, 1992; Escuder-Viruete, 1999). The authors consider two possible kinds of reactions: fluid-absent and fluid-present melting, both of them producing peritectic amphibole plus felsic melt. Experimental studies however give evidence that it was the fluid-present melting of biotite-plagioclase-quartz assemblage which is able to produce amphibole at moderate to high pressure and high temperature (700-750°C/0.3-0.7 GPa, Büsch et al., 1974; 800-900°C/1-2 GPa, Gardien et al., 2000). Amphibole itself is one of the most stable hydroxil-bearing minerals in melting processes (Whitney, 1988). Amphibole coexists with melts at a wide range of *P-T* conditions (850°C/0.2 GPa to 950°C/1.6 GPa) in fluid-absent and water-saturated melting experiments of mafic rocks (Patiño Douce, Beard, 1995; Zharikov, Khodorevskaya, 1997).

Amphibole-bearing leucosomes in the Central Rhodope migmatites are found in amphibole-biotite gneisses from the Vacha River valley (Cherneva et al., 1995), and in amphibole-free biotite gneisses from the Chepelarska River valley (Cherneva et al., 1997). The *P-T* conditions of migmatization there (620-650°C/0.6-0.8 GPa) as estimated by amphibole-plagioclase thermobarometry and garnet-biotite thermometry reflect most probably thermal re-equilibration due to subsolidus ductile deformation. A new find of undeformed amphibole-bearing leucosome from the Chepelare area gave cause for the present study in order to enrich the knowledge of mechanisms and *P-T* conditions of migmatization in the Central Rhodope.

Geological setting and field observations

The outcrop of amphibole-bearing leucosome is situated 3 km to the west of Chepelare town in the northern slope of the Sivkovska river, along the tourist path to the Izgrev hut (Fig. 1a). The studied area belongs to the Arda tectonic unit (Burg et al., 1990; Ivanov et al., 2000) dominated by migmatitic orthogneisses (Cherneva, Georgieva, 2005). The Arda unit comprises a level of dismembered para- and orthometamorphic rocks (graphite-bearing garnet-kyanite gneisses and schists, marbles, garnet-bearing metagabbros, amphibolites, and ultramafics). This variegated rocks assemblage is known as Chepelare formation from the lithostratigraphic subdivisions of the Central Rhodope metamorphic rocks (Ivanov et al., 1984; Khozoukharov, 1984). Recently Sarov et al. (2007) introduced the Chepelare melange designation for the same rock assemblage. Immediately above the latter in the Arda unit section Burg et al. (1990) traced a regional scale ductile shear zone distinguished by mylonitic orthogneisses, enveloping lenses of retrogressed eclogites. The zone is an important component of the syn-metamorphic south-vergent thrust system in the Central Rhodopes (Burg et al., 1996), related to the compressional stage of crustal thickening during the Alpine evolution of the Rhodope massif (Ivanov et al., 2000). In the same zone Dimov et al. (1996)

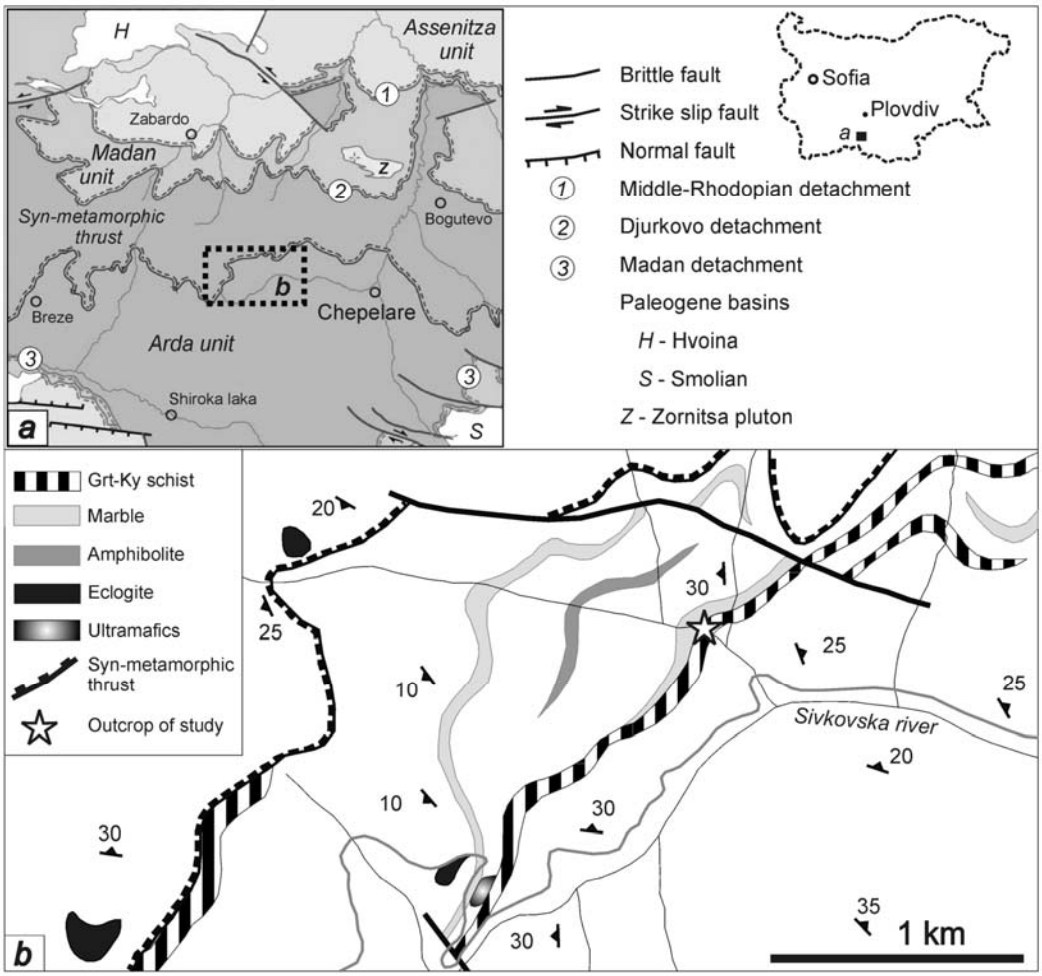

Fig. 1. Tectonic sketch map (a) and geologic map of the area of study (b) after Sarov et al. (2007)

described several mylonitic levels, comprising penetratively deformed migmatites and pegmatites. According to Gerdjikov et al. (2003) considerable ductile deformation is concentrated in the base and into the Chepelare melange as well, which together with the observations of deformed migmatites and pegmatites suggest that crustal thickening was still active during the late syn- to post-migmatitic stage of the metamorphic evolution.

The migmatitic gneiss comprising the amphibole-bearing leucosome is situated among the Chepelare melange rocks (Fig. 1b). The latter occur gently dipping (30-35°) to the west, overlaying two-mica diatexite ortho-gneiss (migmatite terms after Ashworth, 1985, and Wimmenauer and Bryhni, 2007). The diatexite comprises scattered concordant quartz-feldspar leucosome and discordant to the foliation massive granitic leucosome with diffusive contacts. Above the diatexite ortho-gneiss, within about a 50 m long scarp, consecutively crop out two-mica garnet-kyanite schists alternating with felsic garnet-biotite

gneisses, amphibole-biotite gneiss, white marbles, amphibolites, two-mica garnet-kyanite schists, and silicate-bearing marbles. The schists are mica rich and strongly sheared within the first several meters above the diatexite. There the deformation caused considerable reduction of kyanite and garnet grain sizes and nearly complete retrogressive replacement of kyanite by muscovite. Concordant to the foliation quartz-feldspar leucosome bands and elongated lenses indicate initial stage of anatectic migmatization (metatexis) in all gneisses and schists. Mafic minerals are common in the leucosome segregations. In the schists, garnet and kyanite form scarce porphyroblasts inside the leucosome, and coarse-grained biotite rich melanosome selvages. The leucosome of the garnet-biotite gneiss is garnet-bearing and kyanite-free. The leucosome of the amphibole-biotite gneiss contains large amphibole grains. All the silicate rocks are strongly affected by weathering. Fairly intact is the amphibole-bearing leucosome.

The amphibole-bearing coarse-grained to pegmatoid leucosome segregations form bands and elongated lenses 0.5 to 2.5 cm thick, concordant to the foliation of the mesocratic amphibole-biotite host gneiss (Fig. 2a). Scarce syn-migmatization tight folds cause up to 5 cm leucosome thickening. Single euhedral, short prismatic amphibole crystals (up to 2–3 cm, Fig. 2b) occupy the leucosome inside. The leucosome boundaries are distinct though diffuse on a millimeter scale. Sparse clusters of small biotite and amphibole grains form poorly defined melanosome-like selvages 3–4 mm thick. Field observations do not record meso-scale indicators of subsolidus leucosome deformation.

Petrography

The leucosome mineral assemblage comprises major amphibole, plagioclase, K-feldspar, quartz, and minor biotite. The accessory association is dominated by Ca-minerals (apatite, titanite, allanite, and epidote), plus zircon and magnetite. The leucosome matrix (felsic mineral "groundmass", surrounding large amphibole grains) is composed of relatively equal proportions of plagioclase, K-feldspar and quartz.

The amphibole grains are euhedral and optically homogeneous, exhibiting dark bluish-green to greenish-brown pleochroism. Large amphibole crystals are poikilitic, filled with randomly oriented inclusions of euhedral plagioclase and quartz up to 1 mm large (Fig. 3a). The number and size of inclusions

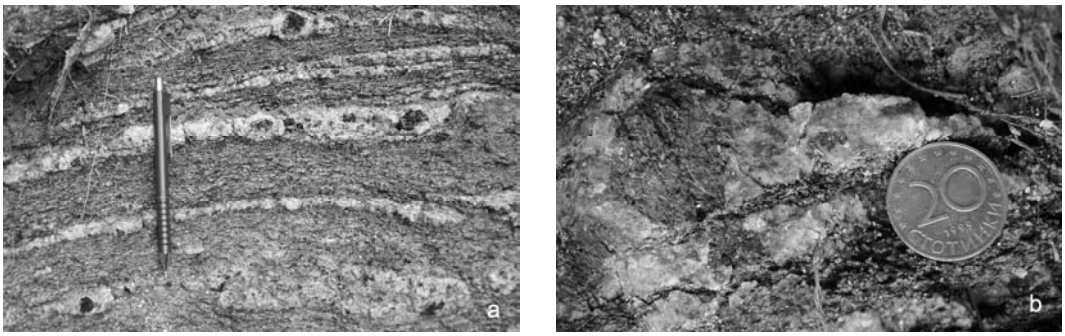

Fig. 2. Concordant to the foliation amphibole-bearing leucosome (pen - 15 cm; coin diameter - 20 mm)

increase toward amphibole periphery. The latter wraps aggregates of subhedral plagioclase, K-feldspar, and quartz (Fig. 3b). Small euhedral to subhedral amphibole grains (1–3 mm, Fig. 3c) are scattered in the leucosome matrix. Sharp and clean amphibole boundaries with plagioclase and quartz inclusions and the absence of any reaction textures indicate textural equilibrium (Fig. 3a-c).

Plagioclase, besides euhedral inclusions in amphibole, forms euhedral and corroded myrmekitic inclusions in K-feldspar (Fig. 3d). A single case of anhedral plagioclase inclusion in amphibole represents most likely a relic phase (Fig. 3e). Subhedral plagioclase is abundant in the leucosome matrix (Fig. 3f). Antiperthitic exsolutions of rectangular and lobate to irregular shapes are common. Fine grained secondary white micas mark weak alteration along plagioclase cleavage planes.

K-feldspar in the matrix is subhedral to anhedral (Fig. 3d, f). Myrmekite reaction rims are locally present in adjacent matrix plagioclase grains. K-feldspar penetrates into amphibole grains along cleavage planes, filling thin fissures (Fig. 4a). Similar penetration of K-feldspar is observed where adjacent plagioclase contains abundant antiperthitic exsolutions.

The quartz grains are euhedral to subhedral when included in amphibole, and anhedral in the leucosome matrix. Lobate and rounded quartz inclusions, though sparse are present in amphibole and feldspars as well. All the quartz grains exhibit remarkable uniform extinction, indicating deformation-free subsolidus leucosome environment.

Euhedral dark brown biotite inclusions are common in K-feldspar grains (Fig. 4b). Secondary reddish-brown biotite forms thin rims in association with magnetite along amphibole boundaries (Fig. 4c) and fills microfissures along amphibole cleavage planes or in the felsic matrix. Most of the biotite grains are occasionally chloritized.

The accessory minerals are abundant. Euhedral and rounded zircon inclusions are common in plagioclase. Apatite inclusions exist in all major minerals. Titanite forms euhedral crystals represented as small inclusions in amphibole and K-feldspar, and as large grains in amphibole periphery (Fig. 3b) and the leucosome matrix. Scanty allanite inclusions in amphibole periphery display euhedral outlines against amphibole and anhedral ones against quartz, plagioclase and K-feldspar. Epidote subhedral to lobate inclusions (Fig. 4f) are common in amphibole and feldspars, where they rarely associate with magnetite. Clusters of lobate epidote grains take place together with secondary white micas in corroded plagioclase inclusions within the matrix K-feldspar. They formed most probably during plagioclase alteration. Single magnetite grains (1-3 μm) or microcrystal aggregates are included in matrix plagioclase. Secondary magnetite predominates in elongated aggregates along amphibole boundaries in association with reddish-brown biotite (Fig. 4c).

The leucosome grain scale textural relations suggest melt crystallization followed by subsolidus alteration influenced by K-rich fluid phase. Inclusions-poor amphibole cores and inclusions-rich peripheries that wrap the aggregates of felsic matrix assemblage testify a simultaneous crystallization of major minerals with some priority to amphibole. The amphibole crystallization caused Mg-Fe-Ca decrease at relatively high K-Na-Al-Si-concentrations in the melt, which formed felsic minerals dominantly. K-feldspar was the last solid phase that crystallized from the melt at solidus *P-T* conditions. Water-rich fluid released after melt crystallization was the most probable agent in subsolidus alteration accompanied by the formation of secondary biotite, magnetite and probably epidote. Some corroded, lobate inclusions of plagioclase, quartz and epidote can be considered as relics of pre-melting assemblage.

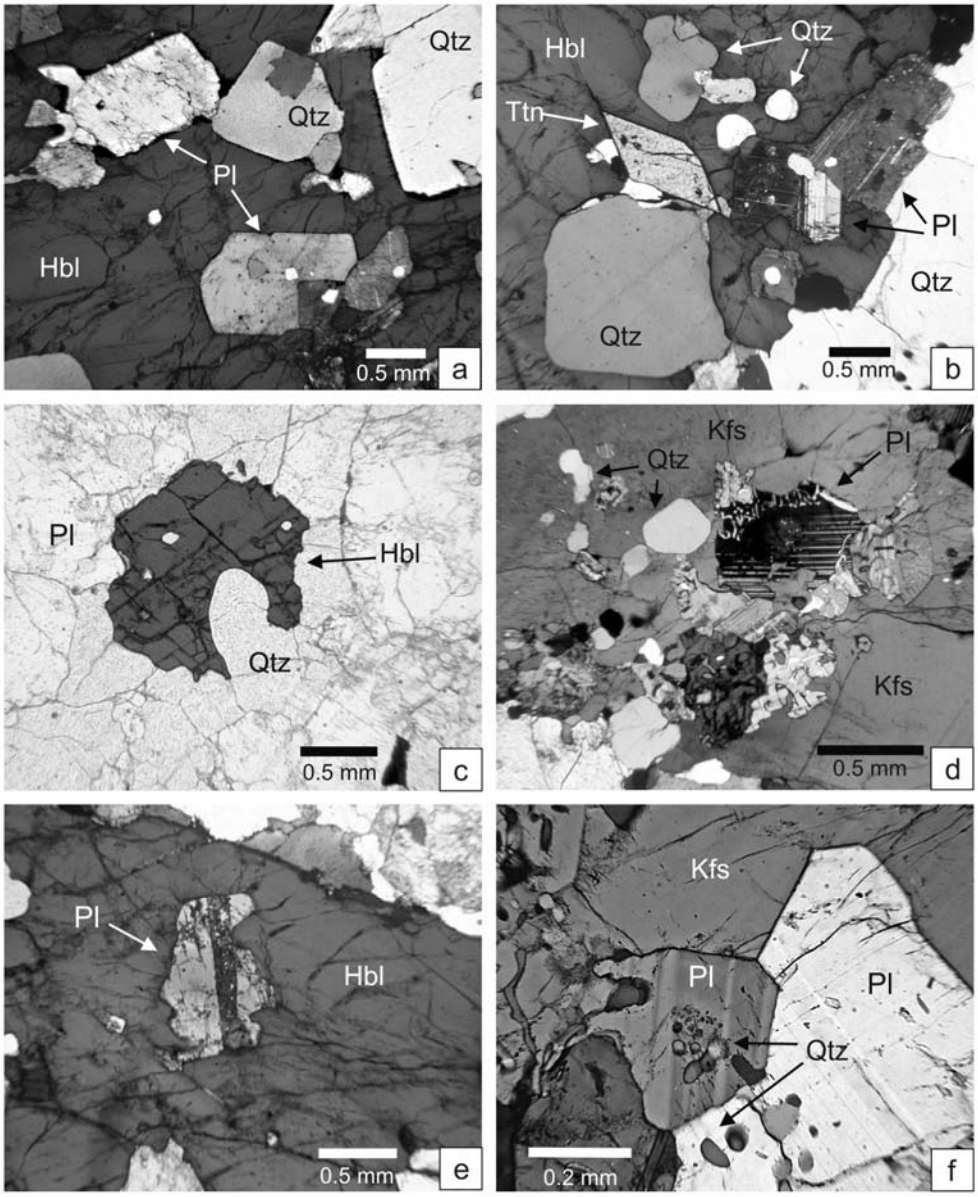

Fig. 3. Poikilitic amphibole with euhedral inclusions of plagioclase and quartz, CPL (a); amphibole rim enveloping euhedral plagioclase, quartz and titanite, CPL (b); subhedral matrix amphibole, PPL (c); euhedral myrmekitic plagioclase inclusions in matrix K-feldspar, CPL (d); anhedral plagioclase (relict?) inclusion in amphibole, CPL (e); subhedral K-feldspar and plagioclase (anti-perthite) in the matrix, CPL (f)

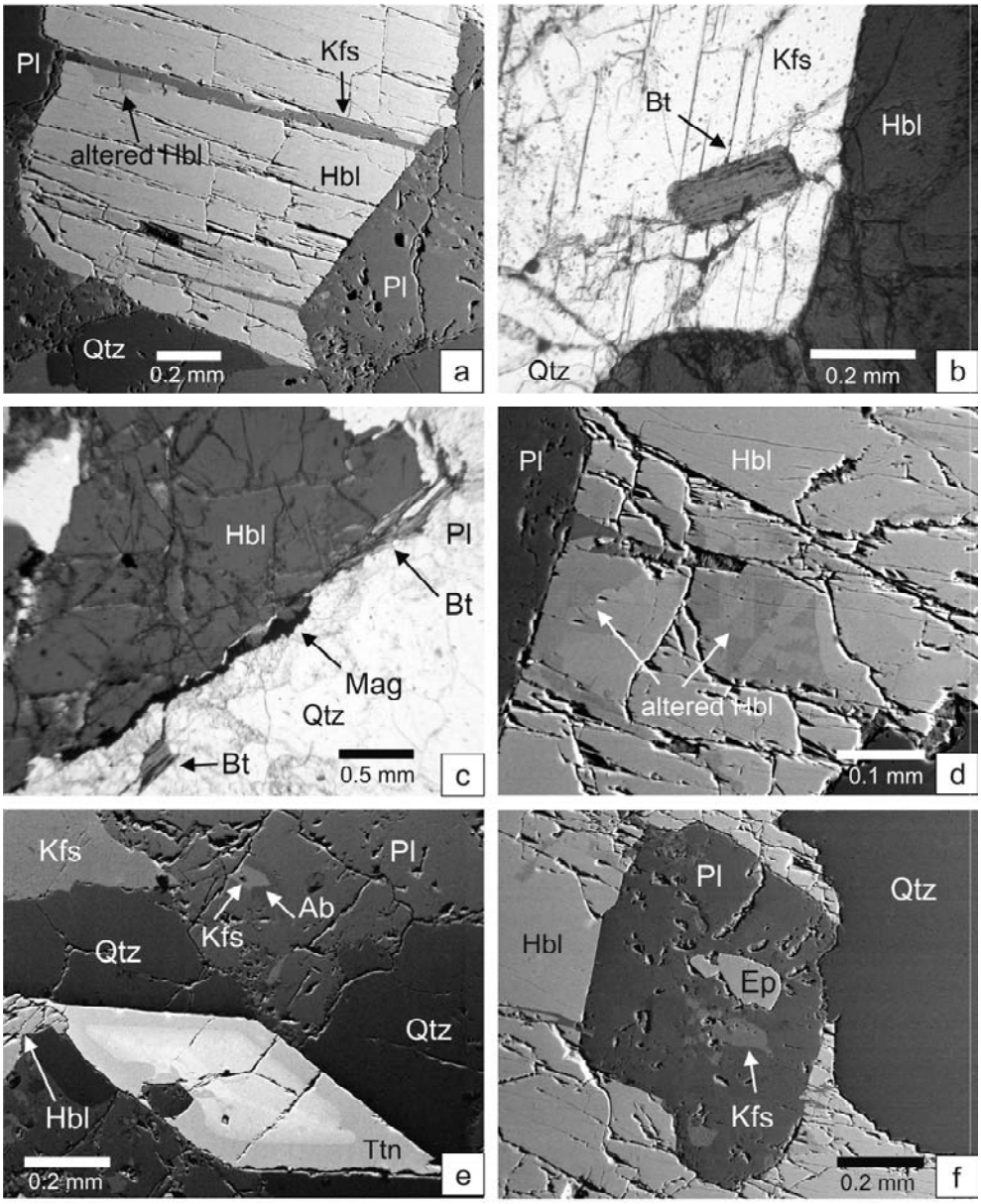

Fig. 4. K-feldspar filling cracks and alteration of amphibole BSE (a); euhedral biotite inclusion in K-feldspar, PPL (b); biotite and magnetite along amphibole margin, PPL (c); patchy amphibole alteration, BSE (d); zoned titanite and anorthite decrease in plagioclase around anti-perthitic exsolutions, BSE (e); subhedral epidote inclusion in plagioclase, BSE (f)

Mineral chemistry

Several samples of amphibole-bearing leucosome were selected for microprobe analyses of the minerals of thermobarometric interest. Analyses were performed on a JEOL Superprobe-733 electron microprobe at the Geological Institute of the Bulgarian Academy of Sciences, with 15 kV accelerating voltage and 100 s counting time.

The amphibole composition (Table 1) corresponds to magnesiohastingsite, hastingsite and tchermakite according to the nomenclature of Leake et al. (1997). Although rather homogeneous, the large crystals display small core to rim decrease of ^{IV}Al and Ti contents, and Mg/(Mg + Fe^{2+}) ratio values (Fig. 5). The amphibole grains in the matrix are similar to large grain rims. The lower ^{IV}Al and Ti contents most likely reflect amphibole equilibration that continued until and ceased at the wet solidus (Schmidt, 1992). The subsolidus alteration caused considerable change in amphibole grains around micro-fissures filled with K-feldspar, and along grain boundaries marked on amphibole BSE images (Fig. 4a, d) by darker areas. The latter correspond to magnesiohornblende and display significant Al, Fe, Ti, Na and K decrease and higher Mg, Ca, and Mg/(Mg + Fe^{2+}) as compared to the fresh amphibole parts (Fig. 5).

Plagioclase compositions range from oligoclase An_{25} to andesine An_{35} (Table 2). Euhedral plagioclase inclusions in amphibole tend to a lower anorthite ($An_{26–32}$), while plagioclase inclusions in matrix K-feldspar are slightly An-enriched ($An_{32–34}$), though both of them lack definite zoning. Matrix plagioclase grains (average An_{30}) display small core to rim differences suggesting reverse zoning. The grain cores are usually lower in anorthite (An_{25-30}) as compared to the rims (An_{28-35}), regardless of the adjacent minerals. The presence of K-feldspar exsolutions, unevenly distributed in plagioclase grains contributes to their compositional inhomogeneity. Data on anorthite reduction (1–2%) in plagioclase around larger exsolutions (visible as darker aureoles on the BSE images, Fig. 4e) confirm such an interpretation.

K-feldspar grains in leucosome matrix and those wrapped in amphibole periphery are similar in composition (Or_{82-88}, Ab_{9-11}, Table 2). The contents of Ba and Ca define low celsiane and anorthite components (Cn_{1-2}, An_{1-3}). K-feldspar exsolutions in plagioclase tend to lower Na and Ba contents ($Or_{85–91}$, Ab_{7-13}, An and Cn ≤ 1). The exsolution amount is about 5 to 10%, estimated by the areas occupied on six plagioclase grain sections. The composition of K-feldspar filling fissures in amphibole grains differ in higher orthoclase ($Or_{94–96}$, Ab_{2-5}), and low An and Cn.

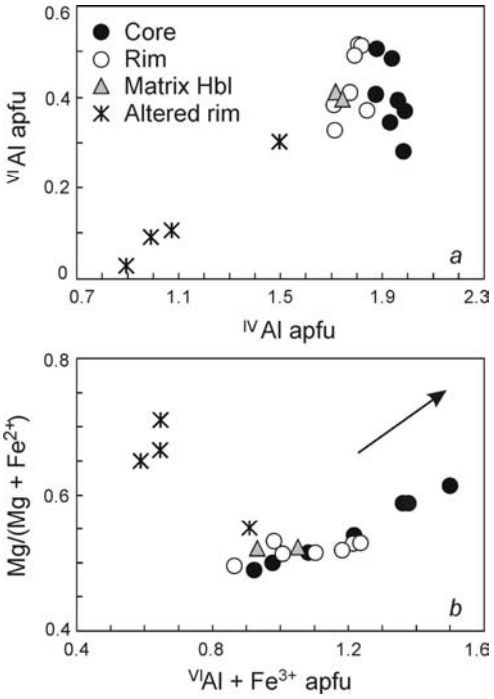

Fig. 5. Plot of amphibole compositions showing: a) slight core-to-rim ^{IV}Al decrease, and total Al-decrease in altered rims; b) core-to-rim variation suggesting tschermakite substitution in amphibole cores (arrow), and total Fe decrease in altered rims

Table 1. *Selected amphibole analyses: cations at 23 O; Fe^{3+} from 13-CNK*

wt.%	Core					Rim			Matrix	Altered rim	
	69c	70c	71c	82c	7c	6r	37r	12r	95	40	41
SiO_2	40.11	40.43	39.56	40.43	39.94	41.45	40.62	40.73	41.70	48.71	47.28
TiO_2	0.94	0.99	0.76	1.16	1.06	0.91	0.95	0.94	0.94	0.55	0.30
Al_2O_3	12.76	13.38	13.17	13.37	13.55	11.71	12.37	12.13	11.99	5.30	6.2
FeO	19.31	19.02	19.02	18.72	18.84	19.80	19.57	19.08	18.84	15.29	16.03
MnO	0.52	0.83	0.76	0.71	0.62	0.68	0.73	0.74	0.75	0.29	0.26
MgO	9.03	9.05	8.95	8.42	8.50	8.45	8.60	8.54	8.96	13.89	12.92
CaO	11.36	11.17	11.60	11.61	11.34	11.92	11.86	11.91	11.92	12.21	12.30
Na_2O	1.30	1.22	1.35	1.37	1.49	0.99	1.55	1.63	1.49	0.85	0.84
K_2O	1.50	1.64	1.41	1.88	1.84	1.25	1.58	1.59	1.50	0.37	0.69
Total	96.83	97.73	96.58	97.67	97.18	97.16	97.83	97.29	98.09	97.46	96.82
apfu											
Si	6.070	6.038	6.012	6.121	6.062	6.290	6.161	6.226	6.283	7.106	7.009
Al	1.930	1.962	1.988	1.879	1.938	1.710	1.839	1.774	1.717	0.894	0.991
T	*8*	*8*	*8*	*8*	*8*	*8*	*8*	*8*	*8*	*8*	*8*
Al	0.346	0.393	0.371	0.507	0.485	0.384	0.372	0.411	0.412	0.018	0.092
Ti	0.107	0.111	0.087	0.132	0.121	0.104	0.108	0.108	0.107	0.060	0.033
Fe^{3+}	1.016	1.106	0.995	0.577	0.729	0.708	0.636	0.453	0.521	0.629	0.554
Fe^{2+}	1.427	1.27	1.422	1.793	1.662	1.804	1.846	1.986	1.853	1.236	1.433
Mn	0.067	0.105	0.098	0.091	0.080	0.087	0.094	0.096	0.096	0.036	0.033
Mg	2.037	2.015	2.028	1.900	1.923	1.912	1.944	1.946	2.013	3.021	2.855
C	*5*	*5*	*5*	*5*	*5*	*5*	*5*	*5*	*5*	*5*	*5*
Ca	1.842	1.787	1.889	1.883	1.844	1.938	1.927	1.950	1.924	1.908	1.953
Na	0.158	0.213	0.111	0.117	0.156	0.062	0.073	0.050	0.076	0.092	0.047
B	*2*	*2*	*2*	*2*	*2*	*2*	*2*	*2*	*2*	*2*	*2*
Na	0.223	0.141	0.286	0.285	0.282	0.229	0.383	0.433	0.359	0.149	0.195
K	0.290	0.312	0.273	0.363	0.356	0.242	0.306	0.310	0.288	0.069	0.130
A	*0.513*	*0.453*	*0.559*	*0.648*	*0.638*	*0.471*	*0.689*	*0.743*	*0.647*	*0.218*	*0.325*
T = 13	13.29	13.32	13.29	13.17	13.21	13.2	13.18	13.13	13.15	13.18	13.16
$Mg/(Mg+Fe^{2+})$	0.59	0.61	0.59	0.52	0.54	0.51	0.51	0.50	0.52	0.71	0.67
Name*	MHs	Tsch	MHs	MHs	MHs	Tsch	MHs	Hs	MHs	MHb	MHb

* MHs – Magnesio-hastingsite; Hs – Hastingsite; Tsch – Tschermakite; MHb – Magnesio-hornblend

Some data on biotite and accessory mineral compositions are shown in Table 3. Biotite euhedral inclusions in K-feldspar display small compositional variations close to phlogopite-annite join in accordance with Al contents (Al^{tot} 2.66–2.81 *apfu*, $^{[IV]}Al$ 2.30–2.50 *apfu*) and Fe/(Fe+Mg) ratio values (0.46–0.50). Titanite euhedral grains, some of which exhibit concentric zoning (Fe enriched core, Fig. 4e), are an important part of the melt-crystallized assemblage. An epidote subhedral inclusion in plagioclase (possible relic phase, Fig. 4f) contains 20–22% epidote component. Magnetite grains situated along amphibole-feldspar boundary and representing most probably a secondary phase contain negligible contents of Si, Mg, Ca и Ti.

Table 2. *Selected analyses of feldspars*

№	SiO_2	Al_2O_3	Fe_2O_3	CaO	BaO	Na_2O	K_2O	Total	X Ab	X Or	X An	X Cn
						Plagioclase						
Single inclusions in amphibole interior												
47c	60.41	25.46	0.12	5.55	-	8.24	0.45	100.23	0.71	0.03	0.26	0.00
49r	60.47	25.50	0.47	5.61	-	8.31	0.30	100.66	0.72	0.02	0.26	0.00
79c	58.45	25.82	0.21	6.74	-	7.57	0.33	99.12	0.66	0.02	0.32	0.00
80r	59.15	26.04	0.42	6.72	-	8.06	0.24	100.63	0.68	0.01	0.31	0.00
Inclusions in amphibole rim												
32c*	59.72	26.29	0.34	6.19	0.10	8.01	0.31	100.96	0.69	0.02	0.29	0.00
35r/hb	60.79	25.09	0.02	5.41	-	8.47	0.21	99.99	0.73	0.01	0.26	0.00
50r/hb	59.64	25.53	0.42	5.97	0.02	8.13	0.28	99.99	0.70	0.02	0.28	0.00
51c*	59.26	25.07	0.16	5.75	0.13	8.19	0.25	98.81	0.71	0.01	0.27	0.00
53r/kf	59.31	25.92	-	6.40	-	7.76	0.29	99.68	0.68	0.02	0.30	0.00
Single inclusons in K-feldspar												
86c	58.11	26.09	0.36	6.99	0.33	7.24	0.33	99.45	0.64	0.02	0.34	0.00
87r	59.17	26.01	0.05	6.69	0.08	7.72	0.28	100.00	0.66	0.02	0.32	0.00
Matrix												
3r/hb	58.46	26.86	0.26	7.18	0.02	7.38	0.25	100.41	0.64	0.01	0.34	0.00
5r/hb	59.24	26.83	0.36	6.74	0.09	7.68	0.26	101.20	0.66	0.01	0.32	0.00
13r	58.17	26.74	0.08	7.20	-	7.42	0.17	99.78	0.64	0.01	0.35	0.00
15c*	59.49	26.07	0.17	5.97	-	8.13	0.34	100.17	0.70	0.02	0.28	0.00
26r/kf	58.69	26.27	-	6.66	0.05	7.57	0.16	99.40	0.67	0.01	0.32	0.00
28c*	57.89	26.99	0.36	7.17	0.14	7.45	0.18	100.18	0.64	0.01	0.34	0.00
46r/hb	59.38	25.44	0.09	5.71	-	7.92	0.53	99.07	0.69	0.03	0.28	0.00
						K-feldspar						
Inclusions in amphibole rim												
54r/pl	64.20	19.67	-	0.18	0.71	1.44	14.41	100.61	0.85	0.13	0.01	0.01
55r/hb	63.58	19.81	0.08	0.22	0.45	1.59	14.61	100.34	0.84	0.14	0.01	0.01
61c	62.95	20.33	-	0.09	0.75	1.88	13.99	99.99	0.82	0.17	0.00	0.01
Matrix												
22c	62.58	19.79	-	0.51	0.44	1.00	15.08	99.40	0.88	0.09	0.02	0.01
23r/pl	62.81	19.52	-	0.21	0.77	1.31	14.18	98.80	0.86	0.12	0.01	0.01
Anti-perthitic exolutions												
1	63.64	19.67	-	0.64	0.03	0.89	15.12	99.99	0.89	0.08	0.03	0.00
14	63.09	19.68	-	0.28	0.53	1.24	14.75	99.57	0.87	0.11	0.01	0.01
27	63.84	19.38	0.04	0.31	0.18	1.18	15.44	100.37	0.88	0.10	0.01	0.00
65	62.98	20.07	0.12	0.22	0.64	1.40	14.42	100.00	0.85	0.13	0.01	0.01
Filling fractures in amphibole												
36	63.11	18.96	0.48	0.29	0.06	0.40	15.99	99.29	0.95	0.04	0.01	0.00
45	63.88	19.19	0.57	0.26	0.23	0.51	16.03	100.67	0.94	0.05	0.01	0.00
48	64.22	19.05	0.34	0.23	0.39	0.28	16.29	100.80	0.96	0.02	0.01	0.01

Note: c – core; c* – anti-perthitic core; r – rim; r/hb, r/kf, and r/pl – rim against amphibole, K-feldspar, and plagioclase respectively

Table 3. *Analyses of biotite and accessory minerals*

Mineral	Biotite		Epidote		Titanite			Magnetite	
wt.%	20	73	38	39	18	76 rim	78 core	9	75
SiO_2	35.88	37.42	36.75	36.63	30.58	30.58	30.15	0.34	-
TiO_2	3.21	3.22	0.23	0.38	38.62	36.96	37.09	0.09	-
Al_2O_3	15.00	14.91	25.93	27.15	1.41	2.25	1.13	-	-
Fe_2O_3	-	-	11.39	10.20	0.71	0.90	1.70	68.19	69.18
FeO	18.99	17.99	-	-	-	-	-	30.89	30.42
MnO	0.17	0.49	0.30	0.36	0.31	0.33	-	-	-
MgO	11.93	11.99	-	0.14	0.09	-	0.22	0.24	0.39
CaO	0.25	0.54	23.12	23.25	28.34	28.97	27.84	0.26	-
Na_2O	0.30	0.42	0.27	0.13	-	-	-	-	-
K_2O	9.63	8.08	-	0.06	-	-	-	-	-
Total	95.36	95.06	97.99	98.30	100.06	99.99	98.13	100.00	100.00

Thermobarometry

The leucosome mineral assemblage offers an opportunity to determine its crystallization *P-T* conditions using amphibole-plagioclase equilibrium pairs. The grain scale textural relationships indicate simultaneous crystallization of amphibole and euhedral plagioclase. Selected pairs (Table 4) represent two types of relations: 1) between Al-enriched amphibole cores and euhedral plagioclase inclusions An_{26-32}; 2) between Al-depleted fresh amphibole rims and subhedral matrix plagioclase An_{32-35}. We expel from consideration the altered amphibole grain parts (magnesiohornblende), distinguished for their strong Al depletion, which are probably not in equilibrium with matrix plagioclase.

The Al/Si ratio values of amphibole-plagioclase pairs are pressure dependent, thus permitting the application of the empirical geobarometer of Ferschtater (1990). The Al/Si values cluster together into two groups of points (Fig. 6), corresponding to higher pressure 0.7–0.8 GPa for the first type and lower pressure ≤ 0.6 GPa for the second type of amphibole-plagioclase pairs.

The mineral association (quartz, plagioclase, K-feldspar, amphibole, biotite, titanite, magnetite) fulfils the requirements of Al-in-hornblende geobarometers (Schmidt, 1992), calibrated experimentally for tonalite and amphibole-bearing granodiorite systems. The equations of Hammerstrom and Zen (1986) and Hollister et al. (1987) yield similar results, with average values approximating those calculated after Schmidt (1992) and shown in Table 4. Obtained pressure values vary from 0.75 to 0.83 GPa for amphibole cores, and from 0.67 to 0.80 GPa for amphibole rims. The lower values in the latter reflect continuous amphibole equilibration until the wet solidus (Schmidt,

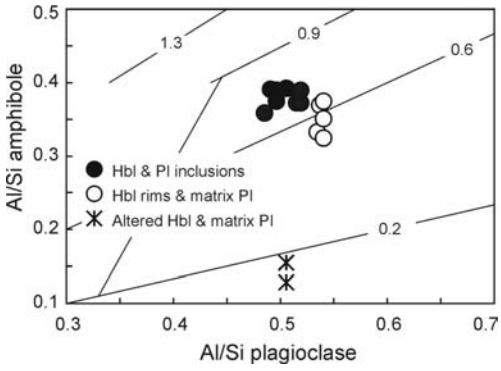

Fig. 6. Empirical geobarometer of Ferschtater (1990) based on Al/Si ratios in amphibole-plagioclase pairs (Table 4). Numbers refer to pressure (GPa)

Table 4. *Thermobarometric estimates of selected amphibole-plagioclase pairs*

Pairs							P GPa Schmidt (1992)	*T*°C (Holland, Blundy, 1994)		
Amphibole				Plagioclase				A (Ed-Tr)	B (Ed-Ri)	*T*°C avrg
№	Al/Si	X Mg	Al tot	№	Al/Si	X An				
Amphibole and plagioclase inclusions										
69c	0.375	0.552	2.28	47c	0.496	0.26	0.78	759	767	763
70c	0.39	0.563	2.36	49r	0.496	0.26	0.82	714	770	742
71c	0.392	0.561	2.36	50r	0.506	0.28	0.82	780	781	781
				51c	0.496	0.27		778	777	778
81c	0.373	0.486	2.28	80r	0.519	0.31	0.79	766	758	762
82c	0.39	0.492	2.39	79c	0.519	0.32	0.83	742	758	750
37r	0.359	0.499	2.21	35r	0.485	0.26	0.75	773	751	762
P avrg							0.80			762
Aamphibole rims and matrix plagioclase										
6r	0.333	0.502	2.09	5r	0.534	0.32	0.70	726	740	733
8r	0.325	0.513	2.04	3r	0.54	0.34	0.67	793	779	786
11r	0.375	0.497	2.32	13r	0.54	0.35	0.80	724	757	741
12r	0.351	0.486	2.19				0.74	788	769	779
P avrg							0.73			760

1992), and concomitant diffusion reequilibration of matrix plagioclase rims (commonly An-enriched). Some subsolidus alteration influence mentioned above, causing Al-depletion of amphibole seems possible as well. Therefore the average value of 0.80 GPa calculated for amphibole cores is an acceptable pressure estimate of leucosome crystallization starting point.

The thermal conditions of leucosome crystallization are calculated according to the amphibole-plagioclase geothermometer of Holland and Blundy (1994) at pressure values obtained after Schmidt (1992), following the requirements and instructions of mineral formula calculations with additional corrections recommended by Dale et al. (2000). The thermometric results range from 714 to 793°C (Table 4). The equation versions (A - edenite-tremolite and B - edenite-richterite after Holland and Blundy, 1994) yield identical average temperatures for the two types of amphibole-plagioclase pairs (762° and 760°C, Table 4, Fig. 7). The average value of 761 ± 21°C could be considered as a starting temperature of leucosome crystallization (amphibole together with plagioclase completely or partially included in amphibole periphery).

The solidus conditions of the leucosome crystallization could be inferred from the matrix assemblage. The presence of euhedral K-feldspar in aggregates with plagioclase and quartz, wrapped by amphibole periphery testify for a simultaneous crystallization of amphibole and the two feldspars at 760°C/0.8 GPa. On the other hand the grain scale textural relations in the matrix indicate that K-feldspar was the last phase that crystallized from the anatectic melt at water-saturated solidus conditions. The latter suggest compositional equilibrium between matrix K-feldspar and plagioclase, disturbed by subsolidus exsolutions. The attempt to apply two-feldspar thermometry (after Fuhrman, Lindsley, 1988), using real feldspar compositions gave satisfactory results for pairs of K-feldspar exolutions (Or_{87-91}) and host plagioclase (An_{28-34}). Obtained concordant temperatures 460°-550°C/0.3-0.7 GPa corroborate the

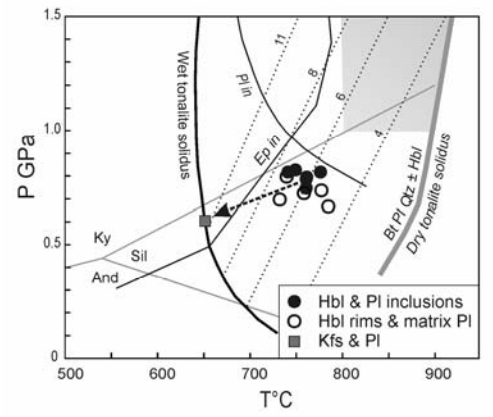

Fig 7. Thermobarometric results for amphibole – plagioclase pairs (Table 4), and K-feldspar – model plagioclase pair (explanation in the text); wet tonalite solidus (Schmidt, 1993); Ep-in and Pl-in curves (Schmidt, Thompson, 1996); dry melting of Bt+Pl+Qtz±Hb = dry tonalite solidus (Patiño Douce, 2005); shaded area corresponds to melting experiment conditions of Bt+Pl+Qtz+H_2O→Hb+melt (Gardien et al., 2000); thin doted lines and numbers refer to minimum H_2O contents (wt.%) of haplogranitic melts (Table 2.3 of Johannes, Holtz, 1996); Ky-Sil-And stability fields (Holdaway, 1971). The arrow shows the amphibole-bearing leucosome crystallization path

interpretation of subsolidus re-equilibration. The approximate estimate of exsolutions amount (5–10%) enables a reconstruction of plagioclase composition. The latter model ($Ab_{65.3}$ $Or_{5.8}$ $An_{28.7}$ $Cn_{0.1}$) is calculated from the average real matrix plagioclase ($Ab_{68.2}$ $Or_{1.5}$ $An_{30.2}$ $Cn_{0.1}$) plus 5% added exsolutions (average $Ab_{10.4}$ $Or_{87.8}$ $An_{1.4}$ $Cn_{0.5}$). The pairs of model plagioclase and the richest in albite K-feldspar cores ($Ab_{15\text{-}17}$, Table 2) yield concordant temperatures 648-658°C at 0.6-0.8 GPa, corresponding to the water-saturated tonalite solidus (Fig. 7).

The combination of thermobarometric estimates define leucosome crystallization *P-T* path from 760˚C/0.8 GPa to 650˚C/0.8-0.6 GPa (Fig. 7), followed by subsolidus re-equilibration of the feldspars at 550-450˚C and lower pressure.

Discussion

Represented data characterize the stage of amphibole-bearing leucosome crystallization. The stage of subsolidus re-equilibration is accompanied by some compositional changes of major minerals in the absence of deformation. The thermobarometric results for the crystallization path from 760˚C/0.8 GPa to 650˚C/0.8-0.6 GPa fall within the sillimanite stability field, close to kyanite-sillimanite boundary (Fig. 7). Similar data, though lower temperature (650-680˚C/0.6-0.8 GPa) is common for migmatitic gneisses (Kostov et al., 1986; Cherneva et al., 1995) and migmatitic metapelites (Georgieva et al., 2002) from the Arda unit in the Central Rhodopes. Most of these migmatites suffered subsolidus ductile deformation and thermal re-equilibration (Cherneva et al., 1997; Georgieva et al., 2002). In contrast, the considered amphibole-bearing leucosome is undeformed, that is a premise for obtaining more reliable information of the migmatization process.

The host gneiss is strongly affected by weathering that hampers petrographic characterization and inferences for reactions of melting. The case studies available relate amphibole growth during migmatization of biotite- and amphibole-biotite gneisses to the following general reactions (abbreviations after Kretz, 1983):

$Bt + Pl + Qtz \rightarrow Hbl + Kfs + melt$ (R1)

fluid-absent melting of amphibole-free substrate at low to moderate pressures 0.3 - 0.7 GPa (Lappin, Hollister, 1980; Kenah, Hollister 1983; Escuder-Viruete, 1999);

$Bt + Pl + Qtz + H_2O \rightarrow Hbl + melt$ (R2)

fluid-present melting of amphibole-free substrate at low to moderate pressure 0.3-0.7 GPa (Kenah, Hollister, 1983; Escuder-Viruete, 1999) or at higher pressure 0.8–1 GPa (Mogk, 1992);

$Hbl_1 + Bt_1 + Pl_1 + Qtz \rightarrow Hbl_2 + Pl_2 \pm Bt_2 + melt$ (R3)

fluid-absent melting of amphibole-bearing

substrate (Shkodzinskiy, 1976; Lappin, Hollister, 1980).

Kenah and Hollister (1983, Fig. 8) deduced the parameters of reactions R1 and R2 at low to moderate pressure (R1: 700°C/0.3 and 725°/0.7 GPa; R2 700°C/0.3-0.7 GPa). Recent studies on fluid-absent melting of the assemblage Bt-Pl-Qtz at a wide range of *P-T* conditions (750°-950°C/1 GPa, Gardien et al., 1995; and 840°-1000°C/0.3–1.5 GPa, Patiño Douce, Beard, 1995) document growth of anhydrous mafic minerals only (orthopyroxene, clinopyroxene, garnet). The melting experiments of Gardien et al. (2000) reproduce a reaction analogous to R2 at 800°-900°C/1–2 GPa giving strong arguments that amphibole growth needs at least 2–4 wt.% H_2O added. The addition of 4 wt.% H_2O corresponds to 6–9 wt.% water dissolved in the melt (Fig. 7) at the conditions of the experiment. Besides amphibole, anhydrous phases as garnet (at 1-2 GPa) and clinopyroxene (at 2 GPa) are present among the products of melting. The authors that inferred R3 (Shkodzinskiy, 1976; Lappin, Hollister, 1980) did not discuss the exact reaction parameters. The wide stability between the water-saturated (Schmidt, 1993) and dry tonalite solidus (Patiño Douce, 2005) is an inherent feature of the mineral assemblage Hbl-Bt-Pl-Qtz (Fig. 7). Yet again the fluid-absent melting experiments of Hbl-Bt-Ep-Pl-Qtz assemblage confirm the appearance of anhydrous minerals (Skjerlie, Johnston, 1996).

The absence of anhydrous mafic minerals as garnet, ortho- and clinopyroxene in the amphibole-bearing leucosome directs to fluid-present melting reactions. Some quartz and plagioclase inclusions are the best candidates for relics of reagents displaying irregular or rounded shapes. Most of the epidote inclusions refer to relic phases as well because of their subhedral shapes. Though grain scale relations would presume crystallization prior or simultaneous with amphibole and plagioclase in the magmatic epidote stability field (>760°C/> 1GPa, Fig. 7), the epidote studied is rather rich in Fe (epidote component 20–22%) compared to the magmatic epidote, expected at such conditions (epidote component < 9%, Schmidt, Thompson, 1996). Hence an assumption of relic epidote, coexisting with tonalite or granodiorite melt is possible to draw.

A process of melting in the epidote stability field (760-800°C/>1 GPa; Fig. 7) corresponds to a transition from high-grade amphibolite to moderate-pressure granulite facies conditions (Thompson, 1990). The migmatization features in the pelitic gneisses and schists corroborate the idea of higher-grade metamorphism and melting than commonly accepted for the Arda unit rocks in the Central Rhodope. The garnet- and kyanite-bearing leucosomes testify for melting reactions involving biotite and kyanite. In the pelitic system these proceed at wide range of pressure values (0.5–1.7 GPa) and high temperature ~ 800°C at fluid-present (Vielzeuf, Holloway, 1988), and 850–900°C at fluid-absent melting (Patiño Douce, Johnston, 1991). Thermobarometric estimations available on garnet-kyanite schists from outcrops east of Chepelare (700-750°C/0.9-1 GPa) reflect retrogressive equilibration due to subsolidus ductile deformation (Georgieva et al., 2003). Some preliminary data on polyphase inclusions of crystallized melt in garnet porphyroblasts presuppose even higher *P-T* values than obtained by conventional thermobarometry (Georgieva et al., 2005). The spatial proximity of migmatitic pelites and gneisses comprising amphibole-bearing leucosome suggests similar conditions of migmatization. A process of fluid-present melting in the stability field of kyanite could therefore explain a growth of peritectic amphibole in a substrate of biotite- or amphibole-biotite gneiss according to reaction R2 and/or a fluid-present version of reaction R3.

On the other hand the amphibole grain-scale relations in the leucosome studied clearly refer to melt crystallization rather than to peritectic growth. The present case and previously observed ones (Cherneva et al., 1995, 1997) focus attention on some additional processes that likely contribute to the formation of amphibole-bearing leucosomes. The latter

occur in migmatitic gneisses, which often display close spatial relations in an outcrop scale with amphibolite bodies, affected by retrogressive biotitizaton along the contacts with the surrounding migmatites. This feature suggests back-reactions between refractory amphibolite and felsic anatectic melts, accompanied by diffusion exchange and Ca, Mg and Fe enrichment into the melt (Khodorevskaya, 2002). The diffusive contribution to amphibole growth in the melt fraction should be effective if assisted by melt migration due to syn-anatectic deformation.

The leucosome morphology (concordant segregations evenly distributed in the gneiss) corresponds to deformation controlled melt fraction segregation and migration at a centimeter to hectometer scale in a host ductile environment (Brown, 1994; Vanderhaerhe, 1999). The studied outcrop is situated in an area distinguished for strong and prolonged syn- to post-anatectic deformation (Dimov et al., 1996; Gerdjikov et al., 2003). The leucosome is nevertheless free of subsolidus deformation. Brown (2001) adduced that deformation of partially molten rocks is accommodated by melt-enhanced granular flow, and volumetric strain is accommodated by melt loss. Therefore, preserved melt crystallization textures indicate that in most places syn-kinematic melt migration was not outlasted by ductile deformation, which concentrated in refractory and melt-free substrate.

Conclusion

The amphibole-bearing leucosomes provide information for better understanding of magmatization and melting in gneiss lithologies. Leucosome segregations, unaffected by post-anatectic ductile deformation preserved melt-crystallization textures and mineral assemblages. Amphibole-plagioclase thermobarometry and two-feldspar thermometry define a *P-T*-path of anatectic melt crystallization in the sillimanite stability field from 760˚C/0.8 GPa to 650˚C/0.8-0.6 GPa. The inferred fluid-present melting reactions involve breakdown of biotite and possibly amphibole at upper amphibolite to moderate-pressure granulite facies transition (>760˚C / > 1 GPa). The above results do not specify a thermal peak of melting. They rather expand the *P-T* conditions of migmatization in the Central Rhodope Arda unit towards a higher-grade facies.

Acknowledgments: The National Science Fund of the Ministry of Education and Science in Bulgaria have supported this work financially, grant SSRAU-ES-05/2005.

References

Ashworth, J.R. 1985. Introduction. In: J.R. Ashworth (Ed.), *Migmatites*. Blackie, Glasgow, 1-35.

Brown, M. 1994. The generation, segregation, ascent and emplacement of granite magma: the migmatite-to-crustally-derived granite connection in thickened orogens. *Earth Sci. Rev*., **36**, 83-130.

Brown, M. 2001. Orogeny, migmatites and leucogranites: A review. *Proc. Indian Acad. Sci*., **110**, 313-336.

Burg, J.-P., Z. Ivanov, L.-E. Ricou, D. Dimov, L. Klain. 1990. Implications of shear-sense criteria for the tectonic evolution of the Central Rhodopes massif, southern Bulgaria. *Geology*, **18**, 451-454.

Burg, J.-P., L.-E. Ricou, Z. Ivanov, I. Godfriaux, D. Dimov, L. Klain. 1996. Syn-metamorphic nappe complex in the Rhodope Massif. Srtucture and kinematics. *Terra Nova*, **8**, 6-15.

Büsch, W., G. Schneider, K.R. Mehnert. 1974. Initial melting at grain boundaries. Part II: melting in rocks of granodioritic, quartzdioritic and tonalitic composition. *N. Jb. Mineral. Mh*., **8**, 345-370.

Cherneva, Z., R. Arnaudova, Tz. Iliev, K. Rekalov. 1997. Feldspar thermometry of migmatic formations from the Central Rhodopes. *Rev. Bulg. Geol. Soc*., **58,** 3, 139-156 (in Bulgarian).

Cherneva, Z., D. Dimov, E. Stancheva, L. Daieva. 1995. Subsolidus and anatectic veins in migmatic gneisses from the Vacha River valley, Central Rhodopes. *Rev. Bulg. Geol. Soc.*, **56**, 3, 91-109 (in Bulgarian).

Cherneva, Z., M. Georgieva. 2005. Metamorphozed Hercynian granitoids in the Alpine structures of the Central Rhodope, Bulgaria: geotectonic position and geochemistry. *Lithos*, **82**, 149-168.

Dale, J., T. Holland, R. Powell. 2000. Hornblende-garnet-plagioclase thermobarometry: a natural assemblage calibration of the thermodynamics of hornblende. *Contrib. Mineral. Petrol*., **140**, 353-362.

Dimov, D., Z. Cherneva, J. Georgiev, S. Arkadakskiy. 1996. Structural position of the migmatic formations and metabasites within the ductile shear zone in the Chepelarska River Valley, north of Chepelare. *Rev. Bulg. Geol. Soc.*, **57**, 3, 47-52 (in Bulgarian).

Escuder-Viruete, J.E. 1999. Hornblende-bearing leucosome development during syn-orogenic crustal extension in the Tormes Gneiss Dome, NW Iberian Massif, Spain. *Lithos*, **46**, 751-772.

Ferschtater, G.B. 1990. Empirical plagioclase-amphibole barometer. *Geochemistry*, **3**, 328-335 (in Russian).

Fuhrman, M.L., D.H. Lindsley. 1988. Ternary-feldspar modeling and thermometry. *Amer. Mineral*., **73**, 201-215.

Gardien, V., A.B. Thompson, D. Grujic, P. Ulmer. 1995. Experimental melting of biotite + plagioclase + quartz ± muscovite assemblages and implications for crustal melting. *J. Geophys. Res*., **100**, B8, 15581-15591.

Gardien, V., A.B. Thompson, P. Ulmer. 2000. Melting of biotite + plagioclase + quartz gneisses: The role of H_2O in the stability of amphibole. *J. Petrol.*, **41**, 651-666.

Georgieva, M., Z. Cherneva, K. Kolcheva, S. Sarov, I. Gerdjikov, E. Voinova. 2002. P-T metamorphic path of sillimanite-bearing schists in an extensional shear zone, Central Rhodopes, Bulgaria. *Geochem. Mineral. Petrol*., **39**, 95-106.

Georgieva, M., A. Mogessie, C. Hauzenberger, A. Proyer, Z. Cherneva. 2003. P-T metamorphic path of garnet-kyanite-bearing schists: Chepelare formation, Central Rhodope, Bulgaria. *Mitt. Österr. Miner. Ges*., **148**,152-153.

Georgieva, M., A. Mogessie, Z. Cherneva. 2005. Mineral needles and melt inclusions in garnet from the Chepelare area, Central Rhodope, Bulgaria. *Mitt. Österr. Miner. Ges*., **150**, 40.

Gerdjikov, I., P. Gautier, Z. Cherneva, D. Kostopoulos. 2003. Tectonic setting of ultra-high-pressure metamorphic rocks from Chepelare area, Central Rhodopes. *Bul. Geol. Soc., Ann. Sci. Con. Geology 2003 Sofia,* Abstracts*,* 44-46.

Hammerstrom, J.M., E.-a. Zen. 1986. Aluminium in hornblende: An empirical igneous geobarometer. *Amer. Mineral*., **71**, 1297-1313.

Holland, T., J. Blundy. 1994. Non-ideal interactions in calcic amphiboles and their bearing on amphibole-plagioclase thermometry. *Contrib. Mineral. Petrol*., **116**, 433-447.

Holdaway, M.J. 1971. Stability of andalusite and the aluminum silicate phase diagram. *Amer. J. Sci*., **271**, 97-131.

Hollister, L.S., G.C. Grissom, E.K. Peters, H.H. Stowell, V.B. Sisson. 1987. Confirmation of the empirical correlation of aluminum in hornblende with pressure of solidification of calcalkaline plutons. *Amer. Mineral.*, **72**, 231-239.

Ivanov, Z., S. Moskovski, K. Kolcheva, D. Dimov, L. Klain. 1984. Geological structure of the Central Rhodopes. I. Lithostratigraphic subdivision and features of the section of metamorphic rocks in the northern parts of Central Rhodopes. *Geol. Balcanica*, **14**, 1, 3-42.

Ivanov, Z., D. Dimov, S. Dobrev, B. Kolkovski, S. Sarov, 2000. Structure, Alpine evolution and mineralizations of the Central Rhodopes area (South Bulgaria). *Guide to Excursion B, ABCD-GEODE Workshop, Borovets, Bulgaria*, 50 p.

Johannes, W., F. Holtz. 1996. *Petrogenesis and Experimental Petrology of Granitic Rocks*. Springer-Verlag Berlin Heidelberg, 335 p.

Kenah, C., L.S. Hollister. 1983. Anatexis in the Central Gneiss Complex, British Columbia. In: M.P. Atherton, A. Gribble (Eds.), *Migmatites, Melting and Metamorphism*. Nantwich: Shiva, 142-162.

Khodorevskaya, L.I. 2002. Diffusional interaction of haplogranite melt with amphibolite (experimental modeling). *Experiment in Geosciences*, **10**, 1, 13-18.

Kostov, I., L. Grozdanov, S. Petrussenko, M. Krasteva, D. Rashkova. 1986. Syn- and post-metamorphic mineralizations in the Central Rhodopes. *Geochem. Mineral. Petrol.*, **20-21**, 25-48 (in Bulgarian).

Kozhoukharov, D. 1984. Lithostratigraphy of Precambrian metamorphic rocks from Rhodope supergroup in the Central Rhodopes. *Geol. Balcanica*, **14**, 1, 43-88.

Kretz, R. 1983. Symbols for rock-forming minerals. *Amer. Mineral.*, **68**, 277-279.

Lappin, A.R., L.S. Hollister. 1980. Partial melting in the Central Gneiss Complex near Prince Rupert, British Columbia. *Amer. J. Sci*., **280**, 518-545.

Leake, B. E. et al. 1997. Nomenclature of amphiboles: report of the Subcommittee on amphiboles of the International Mineralogical

Association, Commission on new minerals and mineral names. *Canad. Mineral*., **35**, 219-246.

Mogk, D.W. 1992. Ductile shearing and magmatization at mid crustal levels in an Archean high grade gneiss belt, northern Gallatin Range, Montana, USA. *J. Metam. Geol*., **10**, 427–438.

Patiño Douce, A. 2005. Vapor-absent melting of tonalite at 15-32 kbar. *J. Petrol.*, **46**, 275-290.

Patiño Douce, A., J.S. Beard. 1995. Dehydration melting of biotite gneiss and quartz amphibolite from 3 to 15 kbar. *J. Petrol.*, **36**, 707-738.

Patiño Douce, A.E., A.D. Johnston. 1991. Phase equilibria and melt productivity in the pelitic system: implications for the origin of peraluminous granitoids and aluminous granulites. *Contrib. Mineral. Petrol*., **107**, 202-218.

Sarov, S. et al. 2007. Geological map of Bulgaria 1: 50 000, Chepelare Map sheet (in press).

Skjerlie, K. P., A.D. Johnston. 1996. Vapour-absent melting from 10 to 20 kbar of crustal rocks that contain multiple hydrous phases: Implications for anatexis in the deep to very deep continental crust and active continental margins. *J. Petrol.*, **37**, 661-691.

Schmidt, M.W. 1992. Amphibole composition in tonalite as a function of pressure: an experimental calibration of the Al-in-hornblende barometer. *Contrib. Mineral. Petrol*., **110**, 304-310.

Schmidt, M.W. 1993. Phase relations and compositions in tonalite as a function of pressure: An experimental study at 650°C. *Amer. J. Sci*., **293**, 1011–1060.

Schmidt, M.W., A.B. Thompson. 1996. Epidote in calc-alkaline magmas: An experimental study of stability, phase relationships, and the role of epidote in magmatic evolution. *Amer. Mineral*., **81**, 462–474.

Shkodzinskiy, W.S. 1976. *Problems of physical-chemical petrology and migmatite genesis*. Novosibirsk, Nauka, 224 p. (in Russian).

Thompson, A.B. 1990. Heat, fluids, and melting in the granulite facies. In: D. Vielzeuf, Ph. Vidal (Eds.), *Granulites and Crustal Evolution*. NATO ASI Series, **311**, Kluwer, Dordrecht, 37-57.

Vanderhaeghe, O. 1999. Pervasive melt migration from migmatites to leucogranite in the Shuswap metamorphic core complex, Canada: control of regional deformation. *Tectonophysics*, **312**, 35-55.

Vielzeuf, D., J.R. Holloway, 1988. Experimental determination of the fluid-absent melting reactions in the pelitic system (Consequences for crustal differentiation). *Contrib. Mineral. Petrol*., **98**, 257-276.

Whitney, J.A. 1988. The origin of granite: The role and source of water in the evolution of granitic magmas. *Geol. Soc. Am. Bull*., **100**, 1886-1897.

Wimmenauer, W., I. Bryhni. 2007. *A systematic nomenclature for metamorphic rocks: 6 Migmatites and related rocks*. A proposal on behalf of the IUGS Subcommission on the Systematics of Metamorphic Rocks. Recommendations, web version of 01.02.2007. SCMR website (www.bgs.ac.uk/scmr/home.htm)

Zharikov, V.A., L.I. Khodorevskaya. 1997. The experimental study of amphibolite melting. *Experiment in Geosciences*, **6**, 1, 11-12.

Accepted April 19, 2007
Приета на 19. 04. 2007 г